Converse magnetoelectric effect via strain-driven magnetization reorientations in ultrathin ferromagnetic films on ferroelectric substrates

N. A. Pertsev
Ioffe Institute and Peter the Great St. Petersburg Polytechnic University, St. Petersburg, Russia
(Received 14 May 2015; published 17 July 2015)

A phenomenological theory is developed for the strain-driven magnetization reorientations occurring in ultrathin ferromagnetic films coupled to ferroelectric substrates experiencing electric-field-induced piezoelectric deformations. The theory takes into account the surface/interface magnetic anisotropy playing an important role in the energetics of such films and first describes the thickness-driven spin reorientation transitions emerging in the presence of substrate-induced lattice strains. Then the threshold and critical intensities of the electric field created in a ferroelectric substrate are calculated, at which different magnetic states acquire the same energy or become unstable in a strained ferromagnetic overlayer. To demonstrate stability ranges of various possible magnetization orientations, we introduce *magnetoelectric orientational diagrams*, where the electric-field intensity and film thickness are employed as two variables. Such diagrams are constructed for ultrathin Ni, Fe, and $Fe_{60}Co_{40}$ films coupled to single crystals of classical and relaxor ferroelectrics. The inspection of these diagrams shows that the use of multiferroic hybrids comprising ultrathin ferromagnetic films significantly enlarges the range of ferroic materials suitable for experimental observations of the strain-mediated converse magnetoelectric effect.

DOI: 10.1103/PhysRevB.92.014416 PACS number(s): 75.85.+t, 75.75.−c, 75.30.Gw, 77.80.−e

I. INTRODUCTION

Ultrathin ferromagnetic films and nanoscale magnetic heterostructures have specific physical properties giving rise to important phenomena useful for various device applications [1–3]. In such films, the magnetization statics and dynamics may be affected strongly by the surface/interface contribution to the magnetic anisotropy. This contribution, in particular, often leads to a thickness-induced spin reorientation transition (SRT) and the appearance of perpendicular-to-plane (PP) magnetization in ultrathin films, multilayers, and magnetic tunnel junctions [4–8]. Since the PP magnetization orientation can be stabilized by the magnetoelastic coupling with substrate-induced lattice strains as well [9], an SRT also may be caused by the relaxation of these strains with increasing film thickness [9–11].

In ferromagnetic films fabricated on ferroelectric substrates, lattice strains can be tuned electrically by applying a voltage to the substrate [12–18]. This tuning results from the voltage-induced substrate deformations, caused by the intrinsic piezoelectric effect [12,13,15], ferroelastic domain switching [17,18] or phase transformations [14], and the strain transfer across the film-substrate interface. Owing to the magnetoelastic coupling, such electrically generated film strains can modify the direction or magnitude of the magnetization, which constitutes a strain-mediated converse magnetoelectric (ME) effect. Importantly, the ME susceptibility characterizing this effect is expected to reach giant values when a strain-driven SRT occurs in the ferromagnetic film under the action of voltage applied to a ferroelectric substrate [19]. However, the critical lattice strains inducing an SRT in a thick film are often not accessible experimentally, as demonstrated by the example of iron [19].

In this paper, we report a phenomenological theory of the strain-mediated converse ME effect displayed by multiferroic hybrids comprising ultrathin ferromagnetic films. The theory allows for the surface/interface anisotropy terms of the second and fourth order and first describes the thickness-induced SRTs occurring in the presence of lattice strains (Sec. II). Then the electric-field intensities necessary for the substrate-driven out-of-plane and in-plane magnetization reorientations are calculated for ultrathin films coupled to ferroelectric substrates experiencing linear piezoelectric deformations (Sec. III). In Sec. IV, we introduce the concept of ME orientational diagrams showing stability ranges of various possible magnetic states in the electric field—film thickness plane and present such diagrams for ultrathin Ni, Fe, and $Fe_{60}Co_{40}$ films coupled to single crystals of classical and relaxor ferroelectrics. Section V summarizes our theoretical results and discusses anticipated applications of multiferroic hybrids in microelectronic devices.

II. ENERGETICS OF ULTRATHIN FERROMAGNETIC FILMS

We focus on single-crystalline ferromagnetic films with thicknesses smaller than the exchange length and nanoscale in-plane (IP) dimensions. Such nanolayers have a single-domain ground state, and a homogeneous spatial distribution may be assumed for the magnetization [1,3]. The energy $\tilde{F}$ per unit area of a ferromagnetic film may be written as a sum of the volume contribution $\tilde{F}_v$ proportional to its thickness t_f and the total specific energy $\tilde{F}_s$ associated with two film surfaces [20]. Since $\tilde{F}_v \sim t_f$, it is convenient to employ the effective volumetric energy density $F = (\tilde{F}_v + \tilde{F}_s)/t_f$ in our calculations. Well below the Curie temperature, where the absolute value M_s of the magnetization $\mathbf{M}$ may be regarded as a fixed quantity at a given temperature, both contributions to F can be described by polynomials in terms of the direction cosines $m_i (i = 1,2,3)$ of the unit vector $\mathbf{m} = \mathbf{M}/M_s$. For (001)-oriented epitaxial films of cubic ferromagnets considered in this work, the polynomial expression for the volume contribution $\tilde{F}_v$, which takes into account the substrate-induced strain effects in the first approximation, has been derived earlier [19,21]. The surface (interfacial) magnetic anisotropy $\tilde{F}_s$ is usually described by the second-order term only [1,2], but the fourth-order terms

may be significant as well [22,23]. Therefore, we write this anisotropy in the form $\tilde{F}_s = K_s m_3^2 + K_{s||} m_1^2 m_2^2 + K_{s\perp}(m_1^2 + m_2^2)m_3^2$, where the direction cosines m_i are defined in the reference frame with the x_1, x_2, and x_3 axes parallel to the [100], [010], and [001] crystallographic axes, respectively. By summing all contributions including the term F_0 independent of the magnetization orientation, we obtain the following relation for the energy density $F(m_i)$:

$$F = F_0 + \left(K_{1||} + \frac{K_{s||}}{t_f}\right)m_1^2 m_2^2 + \left(K_{1\perp} + \frac{K_{s\perp}}{t_f}\right)(m_1^2 + m_2^2)m_3^2 + K_2 m_1^2 m_2^2 m_3^2 + B_1(u_1 m_1^2 + u_2 m_2^2) + B_2 u_6 m_1 m_2$$
$$- B_1\left[\frac{B_1}{6c_{11}} + \frac{c_{12}}{c_{11}}(u_1 + u_2)\right]m_3^2 + \frac{K_s}{t_f}m_3^2 + \frac{1}{2}\mu_0 M_s^2(N_{11}m_1^2 + 2N_{12}m_1 m_2 + N_{22}m_2^2 + N_{33}m_3^2). \quad (1)$$

Here $K_{1||}$, $K_{1\perp}$, and K_2 are the fourth- and sixth-order coefficients defining the "bulk-like" magnetocrystalline anisotropy at fixed strains $\mathbf{u}$, B_1 and B_2 are the coefficients of the magnetoelastic coupling terms of the second order in m_i [24], c_{11} and c_{12} are the elastic stiffnesses at fixed $\mathbf{M}$ (we use the Voigt matrix notation for strains and elastic constants), and N_{ij} form the tensor of demagnetizing factors [25] ($N_{13} = N_{23} = 0$ for ultrathin films). Importantly, two different fourth-order coefficients $K_{1||}$ and $K_{1\perp}$ should be introduced for strained thin films [23] instead of only one coefficient K_1 sufficient for bulk cubic ferromagnets [24], because the isotropic biaxial IP strain lowers the symmetry from cubic to tetragonal. The difference between $K_{1||}$ and $K_{1\perp}$ may be due to the magnetoelastic anisotropy terms of the fourth order in m_i [26] and the presence of additional contribution $B_1^2/(2c_{11}) - B_2^2/(2c_{44})$ to $K_{1\perp}$ caused by the IP film clamping [19]. If other magnetic layers are present in the heterostructure, Eq. (1) should be appended by terms allowing for the magnetostatic interaction with these layers, which can be quantified by an effective interaction field $\mathbf{H}_{\text{int}}$ [21], and the interlayer exchange coupling, such as the Ruderman–Kittel–Kasuya–Yosida (RKKY) interaction in metallic multilayers and the coupling via spin currents in magnetic tunnel junctions [27]. Equilibrium magnetization orientations in strained ultrathin films can generally be found only via numerical minimization of the energy density F. However, important analytical results may be obtained by analyzing the Hessian matrix of the function F rewritten in terms of the polar angle θ and the azimuth angle ϕ defining the magnetization direction in the spherical coordinate system.

In thick films, where the surface contribution to the total magnetic energy is negligible, the magnetization $\mathbf{M}$ in the absence of lattice strains lies in the film plane owing to the out-of-plane shape anisotropy ($N_{33} \gg N_{\alpha\beta}, \alpha, \beta = 1,2$). When the IP shape anisotropy is absent ($N_{11} = N_{22}, N_{12} = 0$), the energetically most favorable directions of $\mathbf{M}$ are parallel to the edges of the unit cell at $K_{1||} = K_1 > 0$ (e.g., in Fe films) and to its face diagonals at $K_1 < 0$ (e.g., in Ni films). These equilibrium directions, however, may change in ultrathin ferromagnetic layers even if an IP orientation is retained, as in the case of positive K_s, because the fourth-order surface magnetic anisotropy renormalizes the coefficient of the term $m_1^2 m_2^2$ in Eq. (1). Indeed, if $K_{1||}$ and $K_{s||}$ have opposite signs, a threshold thickness $t_{\text{IP}} = -K_{s||}/K_{1||}$ may exist, at which this coefficient changes from positive to negative or vice versa. Since $K_{1||} + K_{s||}/t_f > 0$ favors the magnetization orientations along ⟨100⟩ and ⟨010⟩ crystallographic directions while negative values of this sum give preference to the ⟨110⟩ orientations, an SRT between two different IP directions may take place at a certain film thickness, as observed in ultrathin Fe films deposited on GaAs(001) [28]. In the considered case of $N_{11} = N_{22}, N_{12} = 0, u_1 = u_2 = u_6 = 0$, this *in-plane* SRT has the form of abrupt 45° magnetization reorientation on crossing the threshold thickness t_{IP}. Anisotropic lattice strains $u_1 \neq u_2$ and unequal demagnetizing factors $N_{11} \neq N_{22}$ enhance the stability of ⟨100⟩ or ⟨010⟩ magnetization directions and induce deviations from the ⟨110⟩ orientations. Under the conditions $\mu_0 M_s^2 N_{11} + 2B_1 u_1 \leqslant \mu_0 M_s^2 N_{22} + 2B_1 u_2$, $N_{12} = 0$, and $u_6 = 0$ favoring the [100] direction of $\mathbf{M}$, the critical thickness at which this orientation loses stability becomes

$$t_{100}^* = -\frac{K_{s||}}{K_{1||} + B_1(u_2 - u_1) + (1/2)\mu_0 M_s^2(N_{22} - N_{11})}. \quad (2)$$

On the other hand, nonzero shear strains u_6 and demagnetizing factor N_{12} stabilize one of the ⟨110⟩ magnetization orientations and induce deflections from the ⟨100⟩ and ⟨010⟩ ones. As a result, the IP instability of the [110] direction at $\mu_0 M_s^2 N_{12} + B_2 u_6 < 0$ and $\mu_0 M_s^2(N_{11} - N_{22}) = 2B_1(u_2 - u_1)$ takes place at the critical thickness

$$t_{110}^* = -\frac{K_{s||}}{K_{1||} + B_2 u_6 + \mu_0 M_s^2 N_{12}}. \quad (3)$$

Equations (2) and (3) show that t_{100}^* and t_{110}^* may differ strongly from $t_{\text{IP}} = -K_{s||}/K_{1||}$.

The surface magnetic anisotropy and substrate-induced lattice strains can also induce a thickness-driven magnetization reorientation between an IP and PP directions [1–11]. Such *polar* SRT may be continuous (second order) or abrupt (first order), which depends on the relation between the critical thicknesses at which IP and PP directions become unstable [22]. When the magnetization reorientation occurs between [100] and [001] directions, these critical thicknesses are given by the expressions

$$t_{100}^{**} = (K_s + K_{s\perp})\left[\frac{1}{2}\mu_0 M_s^2(N_{11} - N_{33}) + B_1\left(u_1 + \frac{c_{12}}{c_{11}}(u_1 + u_2)\right) - K_{1\perp} + \frac{B_1^2}{6c_{11}}\right]^{-1}, \quad (4)$$

$$t_{001}^{*} = (K_s - K_{s\perp})\left[\frac{1}{2}\mu_0 M_s^2(N_{11} - N_{33}) + B_1\left(u_1 + \frac{c_{12}}{c_{11}}(u_1 + u_2)\right) + K_{1\perp} + \frac{B_1^2}{6c_{11}}\right]^{-1}, \quad (5)$$

which are valid at $\mu_0 M_s^2 N_{11} + 2B_1 u_1 \leqslant \mu_0 M_s^2 N_{22} + 2B_1 u_2$, $N_{12} = 0$, and $u_6 = 0$ only. If the [100] and [001] magnetization directions are stable (or metastable) at thicknesses $t_f < t_{100}^{**}$ and $t_f > t_{001}^{*}$, respectively, the SRT is continuous when $t_{100}^{**} < t_{001}^{*}$ and abrupt at $t_{100}^{**} > t_{001}^{*}$. In the first case, the magnetization gradually rotates between IP and PP orientations in the thickness range $t_{100}^{**} < t_f < t_{001}^{*}$, whereas in the second case two minima coexist in the range $t_{001}^{*} < t_f < t_{100}^{**}$, acquiring the same depth at the threshold thickness

$$t_{\mathrm{SRT}} = K_s \left[\frac{1}{2}\mu_0 M_s^2 (N_{11} - N_{33}) + B_1 \left(u_1 + \frac{c_{12}}{c_{11}}(u_1 + u_2) \right) + \frac{B_1^2}{6c_{11}} \right]^{-1}. \quad (6)$$

Similarly, the first-order SRT happens at $t_{001}^{*} > t_{100}^{**}$ and the second-order one at $t_{001}^{*} < t_{100}^{**}$ when the stability ranges of the [100] and [001] magnetization directions have the form of $t_f > t_{100}^{**}$ and $t_f < t_{001}^{*}$, respectively. Furthermore, the SRT may become a *tricritical* transition in the special case of $t_{100}^{**} = t_{001}^{*}$. The calculation shows that the necessary condition for the size-induced tricritical SRT can be written as $K_{1\perp} + K_{s\perp}/t_{\mathrm{SRT}} = 0$, where t_{SRT} is given by Eq. (6).

When the energetically most favorable IP magnetization orientation is parallel to the [110] crystallographic direction, which may take place only at $\mu_0 M_s^2 (N_{11} - N_{22}) = 2B_1(u_2 - u_1)$ and $\mu_0 M_s^2 N_{12} + B_2 u_6 < 0$, the critical thicknesses become

$$t_{110}^{**} = \left(K_s + K_{s\perp} - \frac{K_{s||}}{2} \right) \left[\frac{1}{2}\mu_0 M_s^2 (N_{11} + N_{12} - N_{33}) + B_1 \left(u_1 + \frac{c_{12}}{c_{11}}(u_1 + u_2) \right) + \frac{1}{2}B_2 u_6 + \frac{K_{1||}}{2} - K_{1\perp} - \frac{K_2}{4} + \frac{B_1^2}{6c_{11}} \right]^{-1}, \quad (7)$$

$$t_{001}^{**} = (K_s - K_{s\perp}) \left[\frac{1}{2}\mu_0 M_s^2 (N_{11} + N_{12} - N_{33}) + B_1 \left(u_1 + \frac{c_{12}}{c_{11}}(u_1 + u_2) \right) + \frac{1}{2}B_2 u_6 + K_{1\perp} + \frac{B_1^2}{6c_{11}} \right]^{-1}. \quad (8)$$

The order of thickness-driven reorientation transition can be determined now by comparing the values of t_{110}^{**} and t_{001}^{**} given by Eqs. (7) and (8) and locating positions of the stability ranges of [110] and [001] magnetization directions with respect to t_{110}^{**} and t_{001}^{**} as explained above. In particular, if these stability ranges overlap, the first-order SRT takes place at the thickness

$$t_{\mathrm{SRT}} = \left(K_s - \frac{K_{s||}}{4} \right) \left[\frac{1}{2}\mu_0 M_s^2 (N_{11} + N_{12} - N_{33}) + B_1 \left(u_1 + \frac{c_{12}}{c_{11}}(u_1 + u_2) \right) + \frac{1}{2}B_2 u_6 + \frac{K_{1||}}{4} + \frac{B_1^2}{6c_{11}} \right]^{-1}. \quad (9)$$

Again, a tricritical SRT may occur at $t_{110}^{**} = t_{001}^{**}$, but the condition for its appearance has the form of $K_{1\perp} - K_{1||}/4 + (K_{s\perp} - K_{s||}/4)/t_{\mathrm{trcr}} + K_2/8 = 0$, where t_{trcr} is given by a relation which differs from Eq. (9) only by the presence of additional term $-K_2/8$ in the square brackets.

Thus, the fourth-order surface/interface magnetic anisotropy may have a significant impact on the equilibrium magnetization orientations and SRTs in ultrathin ferromagnetic films. Mathematically, this effect results from the thickness-dependent renormalization of the coefficients of the fourth-order terms involved in the free energy expansion given by Eq. (1). In films with nanoscale thicknesses, this renormalization may be rather strong, making the discussed coefficients very different from the constants $K_{1||}$ and $K_{1\perp}$ characterizing the bulk-like magnetocrystalline anisotropy of the fourth order. For example, the experimental results obtained recently for the MgO/Fe/MgO heterostructure [29] show that the product of the effective fourth-order anisotropy coefficient and the Fe thickness t_f (equal to $K_{1\perp} t_f + K_{s\perp}$ in our notation) varies linearly with t_f. The extrapolation of this linear dependence to $t_f = 0$ gives a nonzero intercept, which demonstrates that $K_{s\perp} \neq 0$. From the extrapolated value we obtain $K_{s\perp} \approx -9 \times 10^{-5}\,\mathrm{J\,m^{-2}}$ for two Fe/MgO interfaces. The observed slope of the thickness dependence further gives $K_{1\perp} \approx 10^5\,\mathrm{J\,m^{-3}}$, which is close to the bulk fourth-order coefficient $K_1 = 4.85 \times 10^4\,\mathrm{J\,m^{-3}}$ of iron [30]. Hence, the effective anisotropy coefficient $K_{1\perp} + K_{s\perp}/t_f$ goes to zero at the Fe thickness of about 0.9 nm and would be negative at smaller thicknesses. The polar SRT is observed at $t_f = (0.9 \pm 0.1)$ nm and seems to be of the first order [29] so that $K_{1\perp} + K_{s\perp}/t_f$ is apparently positive at $t_f = t_{\mathrm{SRT}}$.

III. STRAIN-DRIVEN MAGNETIZATION REORIENTATIONS IN ULTRATHIN FILMS

Consider now a multiferroic hybrid comprising a ferromagnetic film or heterostructure fabricated on a thick ferroelectric substrate sandwiched between two continuous electrodes. In

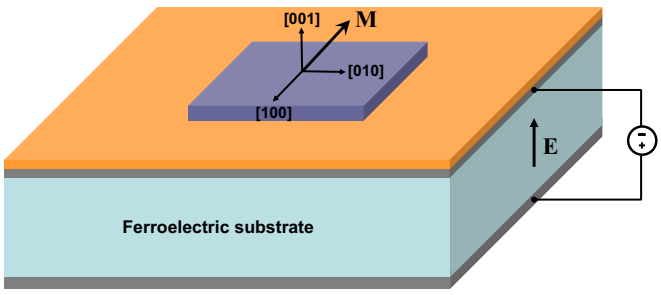

FIG. 1. (Color online) Schematic of a multiferroic hybrid having the form of an ultrathin ferromagnetic layer coupled to a ferroelectric substrate sandwiched between two extended electrodes connected to a voltage source. The spatial orientation of the magnetization **M** may be changed by the electric field **E** creating piezoelectric deformations in the substrate.

this paper, we focus on the most advantageous configuration, where the substrate is covered by the top and bottom electrodes (see Fig. 1) [19]. Connecting these electrodes to a voltage source, one can create a vertical electric field **E** in the substrate ($E_1 = E_2 = 0, E_3 \neq 0$). Owing to the interfacial bonding between the ferromagnetic film and the top electrode or the substrate itself, the field-induced macroscopic piezoelectric deformations of the substrate should change lattice strains in the film. In the linear approximation [19], the in-plane strains involved in Eq. (1) can be written as $u_1 = u_1^0 + \xi_1 d_{31} E_3$, $u_2 = u_2^0 + \xi_2 d_{32} E_3$, and $u_6 = u_6^0 + \xi_6 d_{36} E_3$, where d_{in} are the substrate piezoelectric coefficients in the matrix notation defined in the film reference frame, and $\xi_n \leqslant 1$ are the strain transfer parameters depending on the quality of interfaces. The substitution of these relations into Eq. (1) and the minimization of the resulting free-energy density $F(m_i)$ renders it possible to determine equilibrium magnetization orientations at different field intensities E_3, film thicknesses t_f, and initial lattice strains u_n^0. Hence, the electric-field-induced SRTs can be described quantitatively for multiferroic hybrids, where the strain-mediated effects play the dominant role.

To achieve this goal, we first calculated the threshold field intensities $E_{\rm th}$ at which different magnetic states acquire the same energy in the case of first-order transitions. For the polar SRT between the [100] and [001] magnetization directions occurring at $N_{12} = 0$ and $u_6 = 0$, the calculation yields

$$E_{\rm th} = \frac{\frac{1}{2}\mu_0 M_s^2 (N_{33} - N_{11}) + \frac{K_s}{t_f} - \frac{B_1^2}{6c_{11}} - B_1\left[u_1^0 + \frac{c_{12}}{c_{11}}\left(u_1^0 + u_2^0\right)\right]}{B_1\left[\xi_1 d_{31} + \frac{c_{12}}{c_{11}}(\xi_1 d_{31} + \xi_2 d_{32})\right]}. \tag{10}$$

The threshold field for the magnetization reorientation between the [010] and [001] directions can be found by replacing N_{11} by N_{22} and interchanging d_{31} and d_{32}, ξ_1 and ξ_2, and u_1^0 and u_2^0 in Eq. (10). The inspection of Eq. (10) shows that $E_{\rm th}$ for a polar SRT reduces in hybrids comprising a ferroelectric substrate with high piezoelectric coefficients d_{31} and d_{32} of the same sign. An SRT between IP magnetization directions may be induced by the substrate piezoelectric response as well, but anisotropic film strains $u_1 \neq u_2$ are required for this SRT [31]. The threshold field characterizing the magnetization reorientation between [100] and [010] directions is given by the relation

$$E_{\rm th} = \frac{\mu_0 M_s^2 (N_{22} - N_{11}) + 2B_1\left(u_2^0 - u_1^0\right)}{2B_1(\xi_1 d_{31} - \xi_2 d_{32})}, \tag{11}$$

which demonstrates that the piezoelectric coefficients d_{31} and d_{32} should be opposite is sign to effectively induce this in-plane SRT.

Using the relations for threshold film thicknesses given in Sec. II, we can also clarify the thickness dependence of threshold fields characterizing polar SRTs. In particular, Eq. (10) can be cast into the form

$$E_{\rm th} = -\frac{1}{B_1[\xi_1 d_{31} + (c_{12}/c_{11})(\xi_1 d_{31} + \xi_2 d_{32})]} \times \frac{K_s}{t_{\rm SRT}} \frac{(t_f - t_{\rm SRT})}{t_f}, \tag{12}$$

where $t_{\rm SRT}$ is given by Eq. (6) with u_1 and u_2 set equal to u_1^0 and u_2^0. Similarly, the field $E_{\rm th}$ for a magnetization reorientation between [110] and [001] directions occurring at $\mu_0 M_s^2 (N_{11} - N_{22}) = 2B_1(u_2 - u_1)$ and $\mu_0 M_s^2 N_{12} + B_2 u_6 < 0$ can be written as

$$E_{\rm th} = -\frac{2}{[B_1(1 + 2c_{12}/c_{11})(\xi_1 d_{31} + \xi_2 d_{32}) + B_2 \xi_6 d_{36}]} \times \frac{(K_s - K_{s||}/4)}{t_{\rm SRT}} \frac{(t_f - t_{\rm SRT})}{t_f}, \tag{13}$$

where $t_{\rm SRT}$ is defined by Eq. (9) at the initial lattice strains u_n^0. Importantly, Eqs. (12) and (13) demonstrate that the fields $E_{\rm th}$ become small at the film thicknesses close to the respective threshold thickness $t_{\rm SRT}$. Furthermore, the dependence of $E_{\rm th}$ on the proximity parameter $(t_f - t_{\rm SRT})/t_f$ can be calculated without the knowledge of the interfacial anisotropy constants K_s and $K_{s||}$ because they cancel out with the same constants involved in the relations defining $t_{\rm SRT}$.

Similar results have been obtained for the critical fields $E_{\rm cr}$ making the discussed magnetization orientations unstable. In case of the [100] $\leftrightarrow$ [001] SRTs, the [100] and [001] magnetization directions lose stability at the critical intensities $E_{\rm cr}^*$ and $E_{\rm cr}^{**}$ defined by formulae similar to Eq. (12), which can be obtained by replacing the constant K_s by $K_s + K_{s\perp}$ and $K_s - K_{s\perp}$, respectively, and introducing the thickness t_{100}^{**} given by Eq. (4) or t_{001}^* defined by Eq. (5) instead of $t_{\rm SRT}$. For the [110] $\leftrightarrow$ [001] reorientations, the instabilities of IP and PP magnetization directions arise at the critical fields $E_{\rm cr}^*$ and $E_{\rm cr}^{**}$, which can be calculated using modified versions of Eq. (13), where the multiplier $K_s - K_{s||}/4$ is replaced by $K_s + K_{s\perp} - K_{s||}/2$ and $K_s - K_{s\perp}$, respectively, and the thickness t_{110}^{**} given by Eq. (7) or t_{001}^{**} defined by Eq. (8) is employed in place of $t_{\rm SRT}$. Depending on the relation between $E_{\rm cr}^*$ and $E_{\rm cr}^{**}$, the electrically induced magnetization reorientation may be either gradual or abrupt.

The threshold and critical field intensities characterizing IP magnetization reorientations also go down as the film thickness tends to a corresponding threshold or critical value calculated in Sec. II. For example, the critical field for the instability of the [100] direction induced by anisotropic normal strains $u_1 \neq u_2$ can be written as

$$E_{\rm cr} = -\frac{1}{B_1(\xi_1 d_{31} - \xi_2 d_{32})} \frac{K_{s||}}{t_{100}^*} \frac{(t_f - t_{100}^*)}{t_f}. \tag{14}$$

where t_{100}^* is given by Eq. (2). Further, when the magnetization is initially parallel to the [110] crystallographic direction and the substrate piezoelectric deformations induce significant shear strains u_6 in the film, the initial magnetization direction becomes unstable at the field intensity

$$E_{\rm cr} = -\frac{1}{B_2 \xi_6 d_{36}} \frac{K_{s||}}{t_{110}^*} \frac{(t_f - t_{110}^*)}{t_f}, \tag{15}$$

where t^*_{110} is the critical thickness defined by Eq. (3). It should be emphasized that significant fourth-order IP surface anisotropy is needed to observe easy magnetization reorientations predicted by Eqs. (14) and (15). Indeed, both t^*_{100} and t^*_{110} are directly proportional to the anisotropy constant $K_{s||}$, and they should be larger than the thickness of one monolayer to make drastic reduction of E_{cr} possible.

IV. MAGNETOELECTRIC ORIENTATIONAL DIAGRAMS

To describe the influence of electric field on magnetization orientations in ultrathin ferromagnetic films graphically, in this paper we introduce a *magnetoelectric orientational diagram*, where the electric field applied to ferroelectric substrate and the film thickness are used as two variables. Figures 2 and 3 show such ME diagrams constructed for (001)-oriented Ni and Fe films coupled to ferroelectric substrates inducing isotropic biaxial strains $u_1 = u_2$ in the film plane ($u^0_1 = u^0_2$, $u^0_6 = 0, d_{31} = d_{32}, d_{36} = 0, \xi_1 = \xi_2$). This strain state is created, for instance, by $BaTiO_3$ ($d_{31} = d_{32} \approx -38$ pm/V [32]), $PbTiO_3$ ($d_{31} = d_{32} \approx -26$ pm/V [32]), and $Pb(Zn_{1/3}Nb_{2/3})O_3 - 4.5\%PbTiO_3$ (PZN − 4.5%PT, $d_{31} = d_{32} \approx -1000$ pm/V [33]) single crystals poled along the [001] crystallographic direction oriented perpendicularly to the ferromagnetic overlayer. Since such substrates do not generate anisotropic and shear strains in the film, only a polar SRT can be induced by applied electric field. However, the order of this transition and the structure of ME diagram depend on the interfacial anisotropy constants, which are sensitive to materials in contact with ferromagnetic film.

In the generalized diagrams presented on Figs. 2 and 3, the variables are chosen to be the proximity parameter $(t_f - t^{**}_{001})/t_f$ and the normalized field intensity E_3/E_∞, where the critical thickness t^{**}_{001} is given by Eq. (8) and

$$E_\infty = -\frac{(1/2)\mu_0 M_s^2(N_{11} - N_{33}) + B_1(1 + 2c_{12}/c_{11})u^0_1 + K_{1\perp} + B_1^2/(6c_{11})}{B_1(1 + 2c_{12}/c_{11})\xi_1 d_{31}}. \tag{16}$$

This choice enables us to demonstrate the influence of the proximity to a size-induced polar SRT and to obtain a common diagram for ferromagnetic films fabricated on different piezoelectric substrates. Besides, the critical electric field E^{**}_{cr} making the PP magnetization orientation unstable with respect to rotations toward ⟨110⟩ directions is given by a simple relation $E^{**}_{cr} = E_\infty(t_f - t^{**}_{001})/t_f$ in this case. The determination of other transition lines requires numerical computations, which were performed for Ni/Cu and Fe/MgO bilayers coupled to ferroelectric substrates using the energy minimization based on Newton's method.

For Ni films, initial in-plane strains were set equal to the unrelaxed epitaxial strain $u^0_1 = u^0_2 \cong 2.58\%$ created

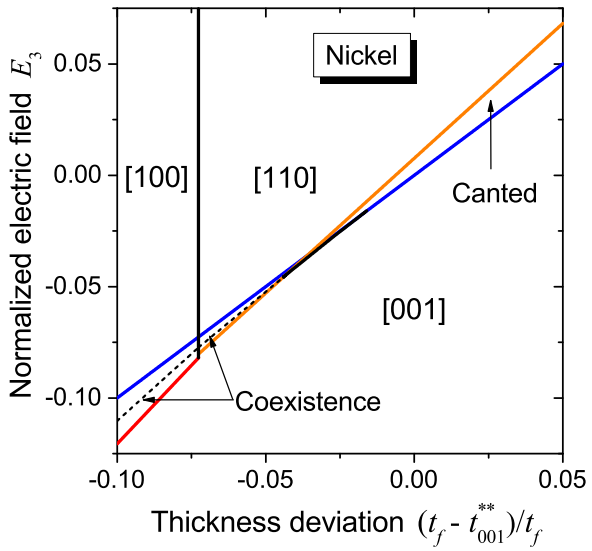

FIG. 2. (Color online) Magnetoelectric orientational diagram of ultrathin Ni films coupled to ferroelectric substrates creating isotropic biaxial strain $u_1 = u_2$ in the film plane. The electric-field intensity E_3 is normalized by the quantity E_∞ given by Eq. (16), and the film thickness t_f is counted from the critical value t^{**}_{001} defined by Eq. (8). The demagnetizing factors and initial lattice strains are assumed to be $N_{11} = N_{22} = N_{12} = 0$, $N_{33} = 1$, and $u^0_1 = u^0_2 = 0.0258$. The dashed line shows the threshold field E_{th} at which the [100] or [110] magnetic state acquires the same energy as the [001] one in the region of their coexistence.

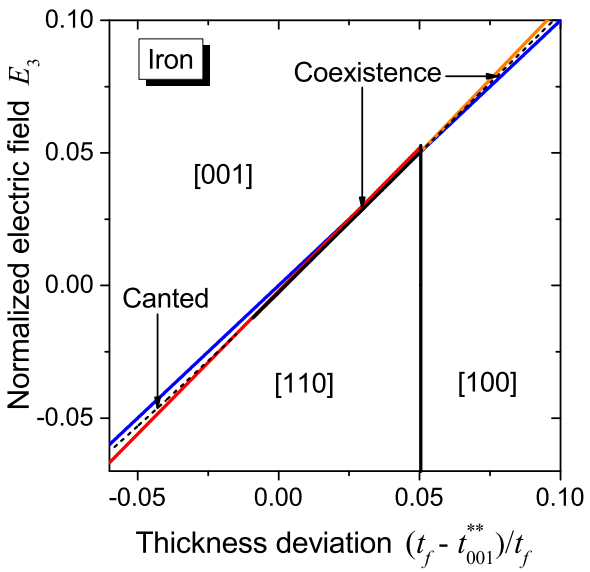

FIG. 3. (Color online) Magnetoelectric orientational diagram of ultrathin Fe films coupled to ferroelectric substrates creating isotropic biaxial strain $u_1 = u_2$ in the film plane. The electric field intensity E_3 is normalized by the quantity E_∞ given by Eq. (16), and the film thickness t_f is counted from the critical value t^{**}_{001} defined by Eq. (8). The demagnetizing factors and initial lattice strains are assumed to be $N_{11} = N_{22} = N_{12} = 0$, $N_{33} = 1$, and $u^0_1 = u^0_2 = 0.039$. The dashed lines show the threshold fields E_{th} at which two different magnetic states acquire the same energy.

in a thin Ni film by a thick (001)-oriented Cu buffer layer. (We assume that lattice strains that may appear in such Cu layer during the growth on a ferroelectric substrate are negligible due to the generation of misfit dislocations at the interface.) The set of fourth-order volume and surface/interfacial anisotropy constants was chosen in accordance with the experimental results obtained for the Ni(001)/Cu(001) heterostructure at the temperature $T \approx 0.8\,T_c$ in Ref. [23]: $K_{1||} = -1.44 \times 10^5\,\mathrm{J\,m^{-3}}$, $K_{1\perp} = -7.26 \times 10^4\,\mathrm{J\,m^{-3}}$, $K_{s||} = 1.98 \times 10^{-4}\,\mathrm{J\,m^{-2}}$, and $K_{s\perp} = 1.02 \times 10^{-4}\,\mathrm{J\,m^{-2}}$. For the second-order anisotropy constant K_s, we used the value of $6 \times 10^{-4}\,\mathrm{J\,m^{-2}}$ corresponding to the combination of the Ni/Cu interface and the clean Ni surface [34]. Other material parameters of nickel were taken to be $M_s = 4.2 \times 10^5\,\mathrm{A\,m^{-1}}$ [23], $B_1 = 9.2 \times 10^6\,\mathrm{J\,m^{-3}}$, $B_2 = 10.2 \times 10^6\,\mathrm{J\,m^{-3}}$, $K_2 = 1.5 \times 10^4\,\mathrm{J\,m^{-3}}$ [30], $c_{11} = 2.465 \times 10^{11}\,\mathrm{N\,m^{-2}}$, and $c_{12} = 1.473 \times 10^{11}\,\mathrm{N\,m^{-2}}$ [35].

The calculations showed that, at the chosen set of parameters, the initial magnetization orientation in the Ni film changes with decreasing thickness from the PP direction to a canted one and then to an IP orientation. This evolution involves gradual magnetization rotation between the [001] direction stable at $t_f > t_{001}^{**} \cong 1.475$ nm and the [110] direction appearing at $t_f < t_{110}^{**} \cong 1.466$ nm. Further decrease in the film thickness down to $t_{\mathrm{IP}} \cong 1.375$ nm is accompanied by a 90° magnetization reorientation into the [100] or [010] direction.

Remarkably, at the Ni thicknesses ranging from t_{110}^{**} to t_{001}^{**}, even a small electric field applied to a ferroelectric substrate should induce an out-of-plane magnetization rotation in the ferromagnetic film. This converse ME effect also exists outside the above range but the necessary field intensity increases as the film thickness deviates from t_{110}^{**} or t_{001}^{**} (see Fig. 2). Interestingly, the region of electric-field-induced canted magnetization orientations in the ME diagram, which narrows with decreasing film thickness, does not disappear when the critical fields E_{cr}^{*} and E_{cr}^{**} providing instabilities of the [110] and [001] magnetization directions become exactly equal at the Ni thickness $t_f \cong 1.423$ nm. This feature is due to the fact that, near this particular point on the ME diagram, the energy minimum of the PP orientation coexists with a deeper minimum, which corresponds to a canted magnetization. As a result, the combination of second- and first-order SRTs appears instead of expected tricritical field-driven transition. At smaller thicknesses, the magnetization reorientation is abrupt (first-order SRT), and a region appears in the ME diagram, where the energy $F(m_i)$ has two coexisting local minima corresponding to IP and PP states.

The ME diagram of Fe films was developed at the initial strains $u_1^0 = u_2^0 \cong 3.9\%$ induced by a thick MgO interlayer and the following set of material parameters: $M_s = 1.7 \times 10^6\,\mathrm{A\,m^{-1}}$ [29], $B_1 = -3.3 \times 10^6\,\mathrm{J\,m^{-3}}$, $B_2 = 10.5 \times 10^6\,\mathrm{J\,m^{-3}}$, $K_2 = 1.5 \times 10^4\,\mathrm{J\,m^{-3}}$ [30], $c_{11} = 2.42 \times 10^{11}\,\mathrm{N\,m^{-2}}$, $c_{12} = 1.465 \times 10^{11}\,\mathrm{N\,m^{-2}}$ [35], $K_s = -9 \times 10^{-4}\,\mathrm{J\,m^{-2}}$, $K_{1||} = K_{1\perp} = 10^5\,\mathrm{J\,m^{-3}}$, and $K_{s||} = K_{s\perp} = -4.5 \times 10^{-5}\,\mathrm{J\,m^{-2}}$. Here we employed the anisotropy constants $K_{1\perp}$, K_s, and $K_{s\perp}$ obtained for the Fe/MgO interface by analyzing the experimental data reported in Ref. [29] with the aid of Eq. (1). As the constant $K_{s||}$ is apparently unknown for this interface, we set $K_{s||} = K_{s\perp}$ because this assumption gives a value of $K_{s||}$, which is close to the experimental one obtained for the Fe/GaAs interface ($K_{s||} \approx -3.5 \times 10^{-5}\,\mathrm{J\,m^{-2}}$ [28]).

Figure 3 demonstrates that the ME diagram of Fe films is basically similar to the Ni one, but the stability ranges of the same magnetic states have different positions in these diagrams (compare Figs. 2 and 3). For the PP magnetization, the difference is due to the fact that this orientation is stabilized in ultrathin Fe films by the interfacial magnetic anisotropy ($K_s < 0$), whereas in Ni films—by tensile lattice strains $u_1^0 = u_2^0$ at $K_s > 0$. Further, the IP magnetization directions along [100] and [110] axes appear at Fe thicknesses above and below t_{IP}, respectively, because the fourth-order anisotropy constants $K_{1||} > 0$ and $K_{s||} < 0$ of iron are opposite in sign to those of nickel. Nevertheless, in both Fe and Ni films the easy axis IP anisotropy transforms into the easy plane one at $t_f = t_{\mathrm{IP}}$, $N_{11} = N_{22}$, and $u_1 = u_2$.

The numerical computations further showed that the loss of stability of the PP orientation always proceeds via the appearance of magnetization component along the [100] or [010] direction. At $t_f > t_{\mathrm{IP}}$, this results in an abrupt reorientation into the corresponding IP magnetic state at decreasing field intensity. In contrast, a canted magnetization appears at smaller thicknesses, being oriented in the (010) or (100) crystallographic plane. Interestingly, under certain conditions, such magnetization direction becomes less energetically favorable than the second possible canted orientation, at which the IP component is parallel to the [110] axis. Therefore, the region of canted orientations in the ME diagram is split into two parts at small film thicknesses and negative electric fields, as demonstrated by dashed line in Fig. 3.

It should be noted that Fe films are not especially suitable for the experimental observation of electric-field-induced magnetization reorientations. Indeed, the characteristic field E_∞ of these films is very high ($E_\infty \approx 2700\,\mathrm{kV/cm}$ for Fe on PZN-4.5%PT), which is due to a relatively low magnetoelastic constant $B_1 \approx -3 \times 10^6\,\mathrm{Jm^{-3}}$ combined with a high magnetization $M_s = 1.7 \times 10^6\,\mathrm{Am^{-1}}$. At the same time, the electric fields applied to ferroelectric substrates cannot exceed the dielectric breakdown field E_b amounting to $\sim 100\,\mathrm{kV/cm}$ for PZN-PT and $Pb(Mn_{1/3}Nb_{2/3})O_3 - PbTiO_3$ (PMN-PT) crystals [36]. Moreover, if the field is applied against the substrate polarization, the field-induced increase in transverse piezoelectric deformations is limited by the ferroelectric coercive field $E_c \sim 2\,\mathrm{kV/cm}$ [36]. As a result, the ME effect in Fe films can be observed experimentally only at thicknesses very close to the critical thickness of the size-driven SRT. However, the range of admissible deviations from this thickness can be increased drastically by using ferromagnetic materials having stronger magnetoelastic interactions. In particular, it is worthwhile to employ $Fe_{1-x}Co_x$ alloys with the Co content $x = 40 - 50\%$, where the magnetoelastic coefficient B_1 rises up to about $-30 \times 10^6\,\mathrm{J\,m^{-3}}$ [37] so that the characteristic intensity E_∞ reduces by an order of magnitude.

Figure 4 demonstrates the ME diagram of ultrathin $Fe_{60}Co_{40}$ films mechanically coupled to the (011)-cut PZN-6%PT single crystal poled along the [011] pseudocubic direction. At this orientation, the PZN-6%PT substrate creates anisotropic strains $u_1 \neq u_2$ in the ferromagnetic overlayer even under vertical electric field because its piezoelectric

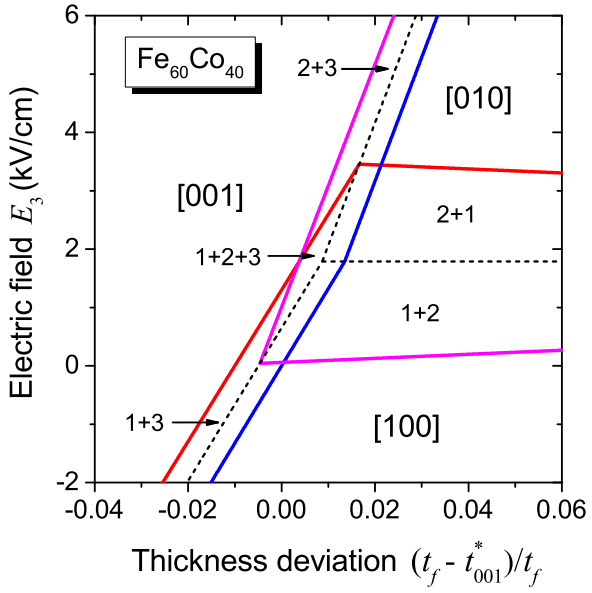

FIG. 4. (Color online) Magnetoelectric diagram demonstrating stable and metastable magnetization orientations in ultrathin $Fe_{60}Co_{40}$ films mechanically coupled to the (011)-cut PZN-6%PT single crystal poled along the [011] pseudocubic direction. The film thickness t_f is counted from the critical value t^*_{001} defined by Eq. (5). The red, magenta, and blue solid lines show the critical electric fields destabilizing the [100] , [010], and [001] magnetization orientations, respectively. The numbers 1, 2, and 3 indicate the coexistence of energy minima corresponding to the [100], [010], and [001] magnetization orientations in the regions bounded by these lines. The dashed lines denote the threshold fields $E_{\rm th}$ at which two coexisting magnetic states acquire the same energy. The demagnetizing factors and initial lattice strains are assumed to be $N_{11} = 0.005$, $N_{22} = 0.01$, $N_{12} = 0$, $N_{33} = 0.985$, and $u^0_1 = u^0_2 = 0$, while the strain transfer parameters ξ_1 and ξ_2 are set to unity.

coefficients d_{31} and d_{32} are opposite in sign ($d_{31} = -3000\,\text{pm/V}$, $d_{32} = 1100\,\text{pm/V}$ [14]). This remarkable feature renders it possible to electrically induce 90° magnetization rotations between different stable orientations in the film plane, which is important for the development of electric-write magnetic memories [31,38]. At the chosen set of material parameters ($M_s = 1.8 \times 10^6\,\text{A m}^{-1}$ [39], $B_1 = -30 \times 10^6\,\text{J m}^{-3}$, $B_2 = -3 \times 10^6\,\text{J m}^{-3}$ [37], $c_{11} = 2.8 \times 10^{11}\,\text{N m}^{-2}$, $c_{12} = 1.4 \times 10^{11}\,\text{N m}^{-2}$ [35], $K_s = -10^{-3}\,\text{J m}^{-2}$ [8], $K_{1||} = K_{1\perp} = -10^4\,\text{J m}^{-3}$, $K_{s||} = K_{s\perp} = 10^{-5}\,\text{J m}^{-2}$ [28], and $K_2 = 0$), such rotations occur between the [100] and [010] crystallographic directions at rather small electric fields of a few kV/cm only, which do not cause the polarization reversal and phase transitions in PZN-6%PT [14]. Interestingly, the critical field intensities for the [100] ↔ [010] magnetization reorientations depend on the film thickness, being defined by the relation $E_{\rm cr} = E_{\rm th} \pm (K_{1||} + K_{s||}/t_f)/[B_1(\xi_1 d_{31} - \xi_2 d_{32})]$, where $E_{\rm th}$ is given by Eq. (11). In the thickness range near the critical thickness t^*_{001} , a polar SRT can be induced in $Fe_{60}Co_{40}$ films as well (see Fig. 4), appearing to be of the first order at the chosen material parameters of the heterostructure.

V. DISCUSSION

In this paper, the strain-driven magnetization reorientations in ultrathin ferromagnetic films have been described theoretically with the full account of the surface/interface magnetic anisotropy. For films coupled to ferroelectric substrates, we analyzed the out-of-plane and in-plane magnetization rotations that may be caused by an electric field created in the substrate sandwiched between two extended electrodes. To this end, the electric-field intensities required for magnetization reorientations have been calculated as a function of the film thickness. It was found that the critical intensities generating out-of-plane magnetization rotations decrease drastically in vicinity of the thickness-induced polar SRT. At the same time, the critical intensities for in-plane magnetization reorientations appear to be only weakly thickness-dependent in the presence of uniaxial in-plane anisotropy, although they also may become negligible at the thickness $t_f = t_{\rm IP}$ if the value of $t_{\rm IP}$ is positive and exceeds one monolayer.

To graphically demonstrate how magnetization orientations vary with the film thickness and electric field created in ferroelectric substrate, we introduced magnetoelectric orientational diagrams, where this thickness and the field intensity are used as two variables. The diagrams developed for multiferroic hybrids comprising Ni, Fe, and $Fe_{60}Co_{40}$ films showed that, depending on the film thickness, the electric field induces either abrupt magnetization reorientations or their gradual rotations (see Figs. 2–4). In both situations, the hybrid displays a strain-mediated converse ME effect, which can be described quantitatively by the susceptibilities $\alpha_{i3} = \mu_0 M_s \delta m_i / E_3$ proportional to the field-induced changes $M_s\,\delta m_i$ in the projections of the magnetization vector $\mathbf{M}$ on the coordinate axes x_i. These ME susceptibilities can be calculated as a function of the film thickness with the aid of the constructed orientational diagrams.

Although the developed theory focuses on films of cubic ferromagnets coupled to substrates experiencing linear piezoelectric deformations, it can be easily generalized on ferromagnetic materials having uniaxial magnetocrystalline anisotropy and on other types of field-induced substrate deformations. Indeed, the uniaxial anisotropy may be incorporated into the theory by renormalizing the demagnetizing factors N_{ij} involved in our relations, while nonlinear and hysteretic substrate deformations resulting from ferroelastic domain switching and phase transformations [14,16–18] can be taken into account by using electric-field dependences of in-plane film strains corresponding to experimentally measured variations of substrate deformations. It should be noted that the theory does not allow for the influence of ferroelectric polarization on the interfacial magnetic anisotropy, which appears in the case of direct contact between ferromagnetic and ferroelectric materials [40] and affects magnetization orientations as well [41]. This approach is justified for hybrids comprising a nonmagnetic interlayer between two ferroic materials, which are considered in this paper, but can be generalized to describe the combined effect of substrate-induced lattice strains and polarization-controlled interfacial magnetic anisotropy. Furthermore, by performing micromagnetic simulations based on the Landau-Lifshitz-Gilbert equation with the effective field allowing for the magnetoelastic coupling one could

evaluate the converse ME effect displayed by hybrids involving ferromagnetic films with large in-plane dimensions, where the initial magnetization distribution may be nonhomogeneous.

The multiferroic hybrids considered in this paper are promising for applications in ME devices. In particular, an abrupt reversible switching of the magnetization between two stable in-plane directions, which is induced by anisotropic strains (Fig. 4), can be employed for the development of an electric-write nonvolatile magnetic memory [31,38]. For a nondestructive readout of two logic states, the multiferroic memory cell should involve a magnetic tunnel junction (MTJ) or multilayer exhibiting giant magnetoresistance (GMR multilayer) instead of a single ferromagnetic layer. Since the electrical resistance of MTJ or GMR multilayer strongly depends on the orientation of the magnetization in the "free" magnetic layer with respect to the magnetization of the "fixed" one [42–44], a reliable readout via resistance measurements becomes possible. It should be emphasized that electric-field-induced resistance variations in GMR multilayers and MTJs fabricated on ferroelectric substrates have been observed experimentally [45,46].

Multiferroic film-substrate hybrids also have important potential applications in electrically tunable microwave devices [14,47]. Since the electric field applied to a ferroelectric substrate changes the film strains and so the magnetoelastic anisotropy, efficient electrostatic tuning of the ferromagnetic resonance (FMR) frequency becomes possible in such hybrids. This feature can be employed to create advanced linear and nonlinear microwave devices with high tuning speed and low energy consumption. Importantly, the electric tunability of FMR frequency should increase drastically near the critical field intensity at which a strain-driven SRT occurs in a ferromagnetic film [47]. Evidently, the existence of size-induced SRTs in ultrathin films provides more opportunities for the realization of such enhancement in tunability. The appearance of gradual field-induced magnetization rotations in the stability ranges of canted states (see Figs. 2 and 3) should affect the electric-field dependence on the FMR frequency additionally.

ACKNOWLEDGMENTS

The work at the Ioffe Institute was supported by the Government of the Russian Federation through the program P220 (Project No. 14.B25.31.0025) and by the Russian Foundation for Basic Research (Grant No. 13-02-12429).

[1] B. Heinrich and J. F. Cochran, Adv. Phys. **42**, 523 (1993).
[2] P. J. Jensen and K. H. Bennemann, Surf. Sci. Rep., **61**, 129 (2006).
[3] F. Vaz, J. A. C. Bland, and G. Lauhoff, Rep. Prog. Phys. **71**, 056501 (2008).
[4] R. Allenspach and A. Bischof, Phys. Rev. Lett. **69**, 3385 (1992).
[5] Z. Q. Qiu, J. Pearson, and S. D. Bader, Phys. Rev. Lett. **70**, 1006 (1993).
[6] J. Moritz, B. Dieny, J. Nozieres, R. van de Veerdonk, T. Crawford, D. Weller, and S. Landis, Appl. Phys. Lett. **86**, 063512 (2005).
[7] J. M. Shaw, S. E. Russek, T. Thomson, M. J. Donahue, B. D. Terris, O. Hellwig, E. Dobisz, and M. L. Schneider, Phys. Rev. B **78**, 024414 (2008).
[8] S. Ikeda, K. Miura, H. Yamamoto, K. Mizunuma, H. D. Gan, M. Endo, S. Kanai, J. Hayakawa, F. Matsukura, and H. Ohno, Nat. Mater. **9**, 721 (2010).
[9] B. Schulz and K. Baberschke, Phys. Rev. B **50**, 13467 (1994).
[10] M.-T. Lin, J. Shen, W. Kuch, H. Jenniches, M. Klaua, C. M. Schneider, and J. Kirschner, Phys. Rev. B **55**, 5886 (1997).
[11] A. Lisfi, C. M. Williams, L. T. Nguyen, J. C. Lodder, A. Coleman, H. Corcoran, A. Johnson, P. Chang, A. Kumar, and W. Morgan, Phys. Rev. B **76**, 054405 (2007).
[12] C. Thiele, K. Dörr, O. Bilani, J. Rödel, and L. Schultz, Phys. Rev. B **75**, 054408 (2007).
[13] A. Brandlmaier, S. Geprägs, M. Weiler, A. Boger, M. Opel, H. Huebl, C. Bihler, M. S. Brandt, B. Botters, D. Grundler, R. Gross, and S. T. B. Goennenwein, Phys. Rev. B **77**, 104445 (2008).
[14] J. Lou, M. Liu, D. Reed, Y. Ren, and N. X. Sun, Adv. Mater. **21**, 4711 (2009).
[15] J.-H. Kim, K.-S. Ryu, J.-W. Jeong, and S.-C. Shin, Appl. Phys. Lett. **97**, 252508 (2010).
[16] T. Wu, A. Bur, W. Kin, Z. Ping, C. S. Lynch, P. K. Amiri, K. L. Wang, and G. P. Carman, Appl. Phys. Lett. **98**, 262504 (2011).
[17] T. H. E. Lahtinen, K. J. A. Franke, and S. van Dijken, Sci. Rep. **2**, 258 (2012).
[18] S. Zhang, Y. G. Zhao, P. S. Li, J. J. Yang, S. Rizwan, J. X. Zhang, J. Seidel, T. L. Qu, Y. J. Yang, Z. L. Luo, Q. He, T. Zou, Q. P. Chen, J.W. Wang, L. F. Yang, Y. Sun, Y. Z. Wu, X. Xiao, X. F. Jin, J. Huang, C. Gao, X. F. Han, and R. Ramesh, Phys. Rev. Lett. **108**, 137203 (2012).
[19] N. A. Pertsev, Phys. Rev. B **78**, 212102 (2008).
[20] U. Gradmann, J. Magn. Magn. Mater. **54–57**, 733 (1986).
[21] N. A. Pertsev and H. Kohlstedt, Adv. Funct. Mater. **22**, 4696 (2012).
[22] H. Fritzsche, J. Kohlhepp, H. J. Elmers, and U. Gradmann, Phys. Rev. B **49**, 15665 (1994).
[23] M. Farle, B. Mirwald-Schulz, A. N. Anisimov, W. Platow and K. Baberschke, Phys. Rev. B **55**, 3708 (1997).
[24] C. Kittel, Rev. Mod. Phys. **21**, 541 (1949).
[25] L. D. Landau, E. M. Lifshitz, and L. P. Pitaevskii, *Electrodynamics of Continuous Media* (Pergamon, Oxford, 1984).
[26] S. V. Vonsowskii, *Magnetism* (Wiley, New York, 1974), Vol. II.
[27] J. C. Slonczewski, Phys. Rev. B **39**, 6995 (1989).
[28] G. Bayreuther, M. Dumm, B. Uhl, R. Meier, and W. Kipferl, J. Appl. Phys. **93**, 8230 (2003).
[29] A. Kozioł-Rachwał, W. Skowroński, T. Ślęzak, D. Wilgocka-Ślęzak, J. Przewoźnik, T. Stobiecki, Q. H. Qin, S. van Dijken, and J. Korecki, J. Appl. Phys. **114**, 224307 (2013).
[30] M. B. Stearns, in *Magnetic Properties of 3d, 4d, and 5d Elements, Alloys and Compounds*, Landolt-Börnstein, New Series, Group III, Vol. 19a (Springer-Verlag, Berlin, 1986).
[31] N. A. Pertsev and H. Kohlstedt, Appl. Phys. Lett. **95**, 163503 (2009).

[32] E. G. Fesenko, V. G. Gavrilyachenko, and A. F. Semenchev, *Domain Structure of Multiaxial Ferroelectric Crystals* (Rostov University Press, Rostov-on-Don, 1990).
[33] J. Yin and W. Cao, J. Appl. Phys. **92**, 444 (2002).
[34] R. Vollmer, Th. Gutjahr-Löser, J. Kirschner, S. van Dijken, and B. Poelsema, Phys. Rev. B **60**, 6277 (1999).
[35] J. P. Hirth and J. Lothe, *Theory of Dislocations* (McGraw-Hill, New York, 1968).
[36] S.-E. Park and T. R. Shrout, J. Appl. Phys. **82**, 1804 (1997).
[37] R. C. Hall, J. Appl. Phys. **31**, S157 (1960).
[38] N. A. Pertsev and H. Kohlstedt, Nanotechnology **21**, 475202 (2010).
[39] I. S. Jacobs, IEEE Trans. Magn. **MAG-21**, 1306 (1985).
[40] C.-G. Duan, J. P.Velev, R. F. Sabirianov, W. N. Mei, S. S. Jaswal, and E. Y. Tsymbal, Appl. Phys. Lett. **92**, 122905 (2008).
[41] N. A. Pertsev, G. Viaud, and B. Dkhil, Phys. Rev. B **90**, 024426 (2014).
[42] M. Julliere, Phys. Lett. A **54**, 225 (1975).
[43] M. N. Baibich, J. M. Broto, A. Fert, F. Nguyen Van Dau, F. Petroff, P. Etienne, G. Creuzet, A. Friederich, and J. Chazelas, Phys. Rev. Lett. **61**, 2472 (1988).
[44] G. Binasch, P. Grünberg, F. Saurenbach, and W. Zinn, Phys. Rev. B **39**, 4828 (1989).
[45] C. Cavaco, M. van Kampen, L. Lagae, and G. Borghs, J. Mater. Res. **22**, 2111 (2007).
[46] P. Li, A. Chen, D. Li, Y. Zhao, S. Zhang, L. Yang, Y. Liu, M. Zhu, H. Zhang, and X. Han, Adv. Mater. **26**, 4320 (2014).
[47] N. A. Pertsev, H. Kohlstedt, and R. Knöchel, Phys. Rev. B **84**, 014423 (2011).